PHYSICAL & VIRTUAL DYNAMIC TEST-BENCH TO APPROACH INTEGRATED SAFETY

Dr.-Ing. Kai-Ulrich Machens, Dr.-Ing. Lars Kübler
ZF Automotive Germany GmbH, Industriestr. 20, 73553 Alfdorf, Germany, Email: *lars.kuebler@zf.com*

Abstract

Achieving the next level of occupant protection requires integrated safety solutions that adapt to the actual driving situation, i.e., expected crash severity, specific information on passengers to guard etc. It will become impossible to cover the increased complexity exclusively by physical vehicle crash tests, as establishing a meaningful holistic safety rating needs many elementary load cases, requiring ultimately a virtual approach. These virtual tools need to include simulation models where the non-linear behavior of all seat belt system (SBS) components caused by crash loads was previously identified and validated by means of reliable and repeatable dynamic subsystem tests. Validating the entire dynamic load map requires a test bench that complies with four fundamentals:

- Matched system dynamics (all key-factors for SBS dynamics addressed)
- Repeatability (generic test configuration database)
- Measurement accuracy (high frequency resolution),
- Efficiency (testing larger number of samples for product characterization).

The innovative test bench Hyper Dynamic Response Actuator (HyDRA®) at ZF in Alfdorf pictured in Figure 1 is driven by nine closed loop controlled electric linear motors moving a rail guided carbon sled along a 6-meter track. Seat belt systems are installed and strapped with high accuracy on generic setups inside mounting frames either connected to the sled or connected to the base. Dynamic forces are built up by a linearly guided free-floating mass acting as inertia source or alternatively by a special Anthropomorphic Test Devices (ATD) seated on the sled. The physical HyDRA® bench is essential for identifying and validating functional SBS simulation models so that simulation becomes its digital twin. An efficient and successful launch of integrated safety systems or rating the effect of Advanced Driver Assistance Systems (ADAS) pre-crash actions is only possible when being able to test the performance of SBS products in an efficient, highly accurate way over the entire range of their functional design space.

Figure 1 **Nine electric linear motors mounted under a carbon-fiber sled and emerged into 6 m long magnet tracks (right-hand picture) powering closed-loop controlled HyDRA® test bench.**

Automotive megatrends call for adaptive safety systems

Automated driving, vehicle electrification and vehicle connectivity can be considered as stable megatrends in today's automotive industry, having in the long run all a major impact on occupant safety solutions.

With increasing level of automated driving the degree of freedom for adjusting the seat will rise, even for the driver, to comfortably pursue non-driving tasks as discussed by Seyffert and Class [1] and Laakmann et al [2]. Automated driving enables new vehicle architectures and alternative mobility concepts giving up the conventional seating position a classical safety system is designed for.

Vehicle electrification is expected to introduce different, probably harder crash pulses due to stiffer vehicle structures to protect the battery packs of electric vehicles, although Justen et al. [3] reported otherwise for their convertible concepts, which integrate an electric drive into conventional body platforms.

Future occupant safety systems need to offer convincing solutions for all these challenges. Most likely these solutions will rely on enhanced pre-crash information made available throughout an extended number of reliable interior and exterior vehicle sensors, allowing to deploy the safety system tailored to any possible use case. The SBS control system selects the optimum response for the actual driving situation, integrating the expected crash severity, specific information on passengers to guard, and the changing vehicle dynamics due to an active intervention from the driver or the Advanced Driver Assistance Systems (ADAS) to avoid or to mitigate the consequences of a potential accident.

Mass and mass distribution of the occupant, and additional physiological passenger properties, i.e. vulnerability captured by the sensory system can be used to choose the optimum restraint strategy for the individuum. Kent et al. [4] reported, that obese Postmortem Human Surrogates (PMHS) show a significant different kinematics compared to non-obese PMHS, expected to result in a different injury risk. A recent investigation by Kroher from ADAC published in [5] raises the question, whether current safety systems validated by EURO NCAP Full Width Crash test provide equal safety for passengers with different physis. They suggest that elderly people are likely to profit most from reduced crash load on the upper body, and they suggest as well that for obese passengers the restraint systems need to be able to deal with higher energy levels than non-obese persons.

The current definition for safety focusing on a few major NCAP and legally required test cases verified by full vehicle conformity tests chould be extended to an integral rating incorporating a variety of different occupants and a multitude of use cases, including pre-crash dynamics (ADAS). This is recognized according to Reuter [6] by the EURO NCAP working group, reported to plan within their roadmap 2030 to extend their rating not only by number of variants of sled tests but to include virtual testing to enhance the robustness of safety system towards the variance of crash severity and occupant physis. Such a safety rating becomes more complex compared to today's rating but is necessary to push occupant safety to the next level and answer the questions of tomorrow. Future systems are expected to be software defined and could be branded as Software-Defined Adaptive Safety (SDAS) Systems. If a crash is expected to happen the SBS control system would select the

appropriate predefined parameter set to drive the safety system based on instantaneous available information for example on the actual driving situation and on the actual seated occupant. The number of significantly varying load cases to establish such a concept is considered by far too complex as to be meaningfully assessed by a limited number of full vehicle tests. Consequently, an alternative validation strategy based on virtual testing is proposed.

Virtual approach anchored in dynamic subcomponent tests

Due to the large variety of different use cases resulting from possible occupants, seating position, crash pulses and dynamic pre-crash activities, illustrated in Figure 2 (left-hand side) and their almost infinite number of combinations, a meaningful holistic safety rating can only be obtained by simulation. Twenty to fifty relevant, full vehicle cornerstone use cases need to be defined and tested in a virtual vehicle environment. Safety ratings are deduced from the simulated occupant loads for each individual use case. An integral safety rating for a vehicle safety system will be obtained by combining the ratings from all relevant use cases.

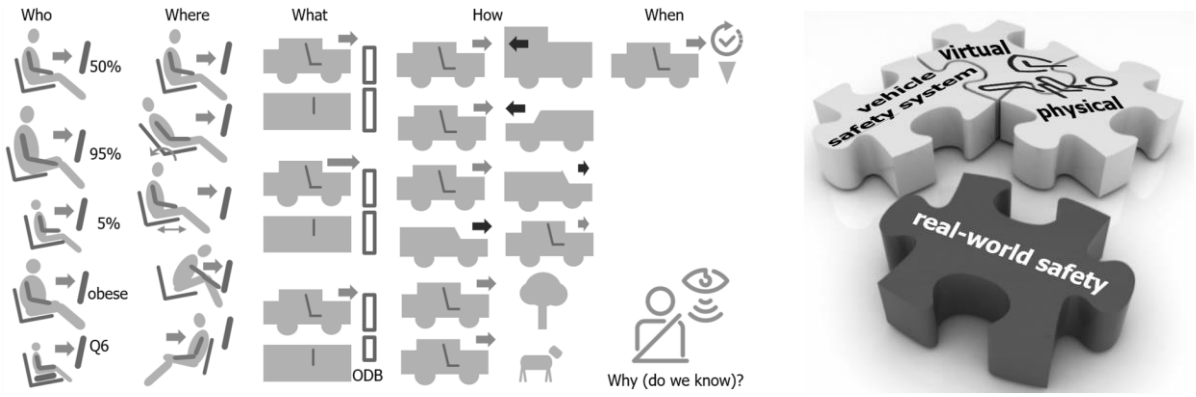

Figure 2 **Left figure: Famous five Ws (and one H)-questions (see [7]) to solve a crime applied to a vehicle accident to demonstrate the complexity of the task to thoroughly validate an adaptive seat belt system. Right figure: Illustration of safety puzzle – physical and virtual bench testing ensure that component functionality fits to simulation model. Once validated the component model becomes part of the full vehicle model to rate the safety system through a multitude of load cases to approach reliable real-world safety.**

Full vehicle simulation, using a mature Anthropomorphic Test Device (ATD) model are known to show reliable results, provided that functional behavior of the major safety components is modeled properly for the load applied. The low pass filter characteristic of ATDs, to be discussed in appendix A, makes virtual full vehicle crashworthiness predictions accessible as the low frequency content can be predicted by simulation with less effort and at higher accuracy. Critical to the prediction quality especially in the first phase of the crash is the high frequency content of the dynamic forces operating on the vehicle side of the belt caused by vehicle pulse and by SBS components activation. This behavior needs to be measured and modelled accurately on sub-system level and incorporated into the full virtual testing model, to ensure proper identification and qualification of SBS functionality on all possible load cases occurring in real-world scenarios.

Functional robustness (quality) is obtained by validating SBS sub-system on multiple dynamic load cases, each with a significant sample size to account for product variability, requiring the test bench to be highly efficient.

Closed loop-controlled E-sled as test bench drivetrain

Focusing on seatbelt systems (SBS), the most interesting and demanding sequence after its activation in a classical accident case is when forces are transmitted to the occupant exclusively via belt and seat / floor. Prior to airbag - ATD contact almost half of the total vehicle crush zone is consumed. In this phase belt pull out is stopped, such that restrain forces build up between passenger and SBS fixation points following the vehicle pulse. Build in load limiting functions will operate either after exceeding a preset load level (CLL) or after a preset time or a preset spool rotation angle controlled active switching (SLL). The seatbelt system is the major element of the energy management on the passenger during this first half of the crash. Only in the second half the load management on the passenger is accompanied by airbags and by deformation work in the seat.

When limiting the analysis to this early seatbelt dominated restrain phase, and when focusing on the accurate loading of the seatbelt system instead of loading the ATD as in traditional crash testing, the required total track length becomes manageable to deploy electronic motors. The total length of the HyDRA® bench and the ability to cycle under full control in both directions allows to bring an inertia source to a defined initial speed first and then reverse the direction of loading such that up to 7.2 m track is available for creating a long deceleration pulse. The available length to shape the pulse on HyDRA® is up to four times longer than the maximum push piston length of 1.7 m of state of the art hydraulicly driven crash devices. Steffan et al. [11] claim that their catapult sled denoted HyperG may be equipped with a special ram to reach strokes of up to 4 m length, but in this case they need to compromise on the force levels and hence possible crash dynamics. This disadvantage is avoided by using linear electric motors as power unit.

With a crush zone of a passenger car typically below 1.5 m the HyDRA® bench, depicted in Figure 1, allows pre and /or post-crash pulse dynamic ac- or deceleration of the carbon sled, and adding of sequences to simulate the dynamic effect of ADAS systems including pre-crash activation of reversible SBS elements. The compactness of the bench in conjunction with moderate payloads allows to use electric linear motors as drivetrain. The HyDRA® bench is equipped with nine linear motors allowing, continuously adjustable speed and positioning control to the nearest millimeter under closed loop control, being the prerequisite to run with a single drive train solution accurately pre-crash maneuvers below 1 g as well as highly dynamic crash pulses with up to $a = 70\ g$ and jerks up to ${}^{\Delta a}/_{\Delta t} = 25000\ g\ s^{-1}$. The maximum acceleration that can be applied at the bench is limited by the maximal propulsion force of the motors and by the payload. Consequently, great attention was paid to light weight design of all moving parts, with the sled itself being made of carbon, and the frames to be attached to the sled, are machined from solid aluminum blocks.

The low inertia of the sled and its attached frames and fixtures, by a factor of 10 lower than on conventional crash sleds, makes HyDRA® sensitive to load changes acting on the moving sled. Pretensioning, locking as well as attaining or switching between load levels will highly dynamically alter the effective sled inertia. To maintain the sled acceleration according to the target pulse these dynamic inertia changes need to be compensated by a highly dynamic closed loop control system. For this purpose, HyDRA® is equipped with a newly developed

control unit working at 8 kHz control frequency, enabling a closed loop control of the nine linear motors with a fast reaction time. Also, the motors provide sufficient power to swiftly compensate all relevant pay load change. The forces that are operating on the moving parts were accounted for by design up front, but some bench components needed a special treatment to withstand the high dynamic forces acting upon, when the sled moves within the parameter set of its design. One example is the so-called energy chain, which runs in a housing at the rear of the bench to supply the power to the E-motors which are placed underneath the sled.

The bare sled is ready to test parts to high dynamic loads by simply mounting the specimens onto it. But the bench is named **Hy**per **D**ynamic **R**esponse **A**ctuator (HyDRA®) from its ultimate purpose to test SBS configuration under conditions simulating the crash response, like mounted in the vehicle and loaded by the response of an ATD. Therefore, special sets of mounting platforms were developed allowing to root and strap the SBS inside a frame. Basic configurations will be discussed in the following paragraphs.

Generic setups based on lumped parameters

One of the basic ideas of the HyDRA® bench is the ability to build an accurate digital twin of the bench, thus being able to validate the dynamic responses of the physical or the virtual seatbelt system by obtaining an equivalent result from the corresponding twin. The webbing, with its mass distribution, and its visco-elasto-plastic stress vs. strain behavior, links mechanically the ATD to the vehicle fixation points. The mass of the webbing for instance causes significant forces to act on the pretensioner when the belt is almost instantly accelerated by 1000-6000 g to a pull-in speed of 20-30 m/s in the pretensioning phase as illustrated in appendix A. In a real vehicle configuration, it is very demanding or almost impossible to control the relevant parameters defining the dynamic resistance for the pretensioner. These parameters are the distributed belt friction along its course from the D-Ring, via the ATD body, trough the buckle into the anchor, the initial conditions i.e., belt to seat contact, initial buckle and anchor position and orientation and especially the distributed slack generated by the seatbelt routing at pelvis and chest. In virtual testing these parameters are assumed to be within a certain range, and it is common practice to freely explore the parameter range selecting the values in a way so that the simulation model output fits results of the physical test. This procedure is justifiable by the little control one has on the actual test parameters. But the predicative capacity of component function simulation models, identified and validated on fuzzy test setups and on small number of dynamically similar load cases is rather limited.
The fuzzy character of these parameters can be taken out of the equation by strapping the seatbelt webbing around fixed aluminum pillars with a defined routing as illustrated in Figure 3. Dependent on the individual routing path, the friction is well defined and proportional to the total wrapping angle as suggested by the capstan equation according [9]. The basic HyDRA® setup, intended for high precision measurements, allows the utilization of different masses, serving as inertia source guided by ball bearings alongside mounted rails depicted in Figure 3 (left-hand and right-hand side). The belt can either be fixed with one end to the mass, (directly pulled mass) or looped around one or two pillars mounted on the mass (looped mass) changing the inertia load by about a factor of two.

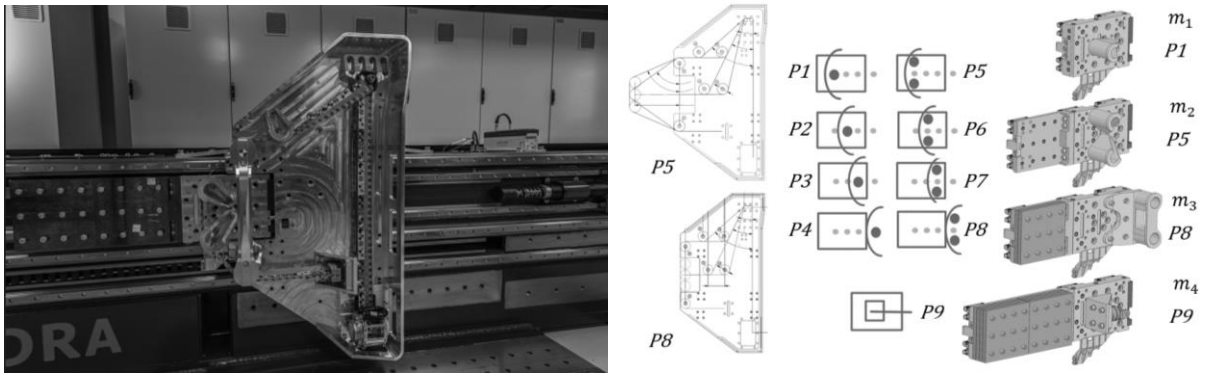

Figure 3 **A lumped mass is guided by ball bearings along straight rails mounted at the side of the bench to realize inertia loading onto the belt (left picture). The total mass can be adjusted (right picture). By anchoring the belt end at the mass or by looping the belt around one or two pillars mounted on the mass significant different loading path of the belt can be applied (central picture). By varying the position of the pillars P1-P9 on the mass the kinematic onset (load change with distance change) is varied. Different routing of the belt changes the friction between belt and pillar dependent on total wrap angle.**

The so-called kinematic onset is an important parameter for looped mass setup. It can be precisely adjusted by the number of pillars mounted, (one or two), as well as by their positioning (one to four) on the mass. Figure 3 in the center illustrates two different initial loading kinematics, with the orientation of the belt routed back and forth to the frame defining how the inertia is connected dynamically via the belt to the load frame in the initial coupling phase. This parameter was introduced to emulate a full occupant behavior of the SBS with a generic setup, one lumped mass only connected at a single point to the SBS, instead of a distributed multibody system with multiple contact points to the SBS along the webbing. This multiple point contact defines how the occupant builds up forces trapped in the locked SBS which can be interpreted as an onset. The discussed setup parameters allow to create an equivalent onset on the bench for different occupant sizes represented by different ATD models (like H305, H350, H395, …) and different seating configurations. The fourth and last element which needs to be considered is slack. A slack element introduces locally a defined amount of slack accounting for the distributed slack in a real-world system, as described in the beginning of this section.

At first glance the concentrated parameter setup could be seen somehow as a shortcoming to the more complex real-world seatbelt system strapped around an ATD in a full scale sled or crash test. If the number of variations in real-world safety systems simply due to the diversity of human bodies being potential passengers is considered, the focus might be moved from trying to copy a singular sled test case with one ATD to a more general and extended approach on HyDRA®. A generic dynamic validation methodology requires the seatbelt system to be tested in a multitude of defined corner stone use cases all to be performed at high reliability, fostered by the availability of an accurate dynamic measurement technology, on the compact HyDRA® bench. Besides high level of control and repeatability of generic test bench configurations, they can be easily cast into a simulation model at high accuracy, being most likely the top advantage of the generic setups, allowing to model, identify and validate functional models, so that all corner stone load cases of the seatbelt system can be performed with validated functional simulations on the digital twin bench.

High precision setup with fixed frame & controlled loading

This setup is inspired from a so-called Linear Impactor Test Bench patent-registered in 1999 by Bock et al. [10],[11] used to evaluate the dynamic behavior of airbags, where a linearly guided mass is propelled at constant speed into an unfolding airbag. Similarly, the present test bench traps and slows down a linear guided free-floating mass driven into a seat belt system. The setup consists of two solid, and stiff frames as depicted in Figure 4: The first frame to mount the retractor at various installation angles and to accommodate D-rings or other belt redirecting devices with build in force gauges. The second frame allows for variable routing of the webbing, such that friction and kinematic onset can be adjusted, and the relative position between the frames sets the total webbing length. In starting position, the free-floating mass, with the weight adjustable between 5-70 kg as previously described, is located between the two frames. A hook attached to the sled as visible on the right-hand side photo of Figure 4 serves as driving dog for the mass. Being placed at the top of a slide mounted to the base the hook is at equal height with a push bar which is part of the free-floating mass. By accelerating the sled, the hook drives the mass displacing and accelerating it towards the belt and decouples the mass from the sled before it establishes contact with the belt. Hereinafter the energized mass is slowed down by the SBS but its displacement is stopped ultimately by one of two bumpers, either the one behind the first static frame visible on the left-hand side photo of Figure 4 or another located at the end of the track (see Figure 1).

Figure 4 **Linear guided mass, coupled to the sled, is first accelerated to a defined speed and then either be decoupled to impact as a free-floating mass on the seatbelt system (see decoupling mechanism on right picture) or stay coupled to be driven displacement controlled into it to load the SBS. The Seatbelt is strapped into two stiff static frames, mounted at the base of the bench. Seatbelt retractors, with engaged locking mechanism, can be mounted in various mounting positions via adaptors to the first base.**

The kinetic energy of the inertia source, which needs to be absorbed by the energy management systems in the SBS, can be adapted by setting the combination of total free-floating mass and impacting speed. The natural response to the forces from the belt system remains nevertheless the natural response of a free-floating mass, which reacts to the forces from the belt system like an ATD strapped in a SBS and run down by the SBS's energy management. Pretensioning, retractor locking, transition to first load limiting level and the switching of load limiting levels can be tested with this setup at high precision and over a large range of kinetic energy levels. Thereby the whole functional design space can be efficiently identified, validated, and cast in a virtual functional model, most accurately when webbing pull-out displacement and speed over time, as well as the corresponding force gradient in the webbing leaving the pretensioner retractor displays the same characteristics as in full vehicle real-world crash scenarios.

The high precision setup with static frame has two major advantages compared to the ones with a moving frame to be discussed in the following section. Firstly, stiff static frames mounted to the compact HyDRA® base have significantly higher structural eigenfrequencies than sled mounted structures. This allows dynamic forces and displacements to be measured with a higher accuracy i.e., a sharper time sequence characteristic. The low noise time sequences allow to conclude to the functioning of inner components, like snake-turbine interaction in a snake retractor pretensioner, or like the response time of a load limiter system inside a retractor. On top of that, since the seatbelt system remains stationary, all relevant details can be captured with non-ruggedized high precision high-speed cameras placed on the laboratory floor, which allow to track relative displacements by postprocessing software accurately. Secondly the possibility to keep the mass coupled to the sled and to run the test in closed-loop displacement controlled into the strapped seatbelt system. Thereby highly repeatable load characteristics, which can be tailored by purposeful variation for each individual investigation, can be run especially supporting the development and optimization of SBS energy management systems. The powerful high dynamic sled can exercise load variation as expected in real world crash scenarios, for example reduced belt pullout velocity caused by occupant – airbag contact.

However, the static frame scenario has the disadvantage, that the seatbelt system is not subjected to the decelerations occurring in a crash and to preconditioning of the SBS from pre-crash activities. These features are addressed by the moving frame scenario discussed next.

Moving frame for testing SBS enduring a crash pulse

A vehicle safety system fitted to the vehicle structure is stressed by the deceleration from the crash pulse and by forces resulting from its crash activation. Moving frames, now coupled to the sled, enable to simulate such a superimposed loading experimentally, with the SBS mounted and strapped either in a front seat frame (Figure 5 right-hand side) or in a back seat frame. Frame and SBS are subjected to the crash pulse slowing down the linear motion of the strapped SBS proving that high dynamic accelerations do not have an effect on the SBS

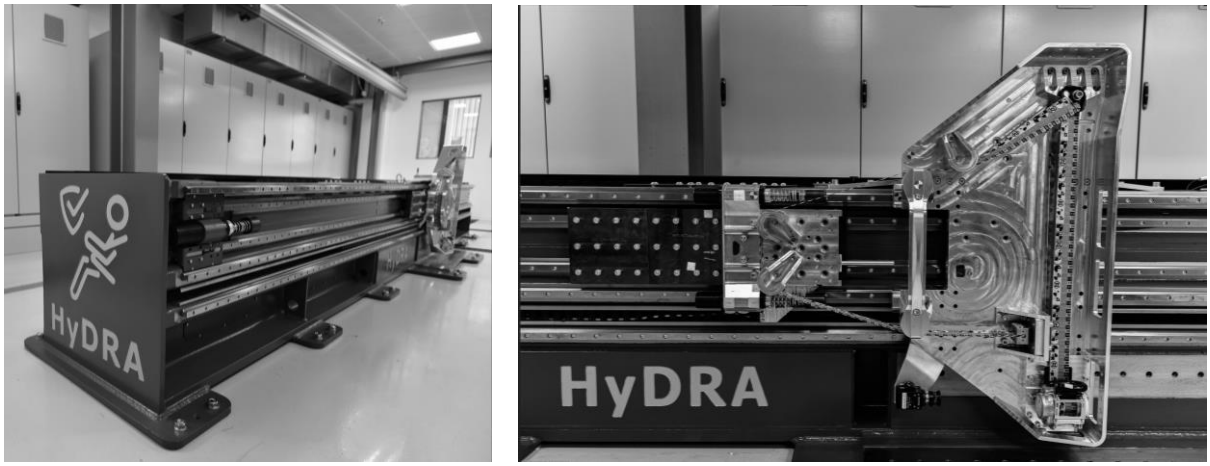

Figure 5 **Front seat frame (right hand) coupled to the sled and guided in ball bearings along the three outer rails visible aside of the bench. A free-floating mass is guided along the two inner tracks, which are set back into the base such that two dampers, fixed to the base, hit the mass in its center to stop it. Beyond the central damper is a safe harbor for the frame, which cannot be reached by the free-floating mass. Alternatively, the frames may also be used to stop the free-floating mass, which is equipped with two additional dampers. An onboard high-speed camara is mounted on the frame to monitor the retractor behaviour.**

restraining function. Each of the moving SBS frames is mounted on six linear ball bearing cages, which are running along three parallel, straight rails at the side of the bench base. The frame designs are the outcome of CAE and optimization work, yielding an optimum solution in terms of lightweight, stiffness, and robustness to cope best with all possible dynamic loads, with the frames being machined from solid aluminum blocks. The milling pattern, visible in Figure 5, are a measure of quality, and the achieved stiffness frames is demonstrated by the first eigenfrequency above 300 Hz. Low mass on the sled is important to achieve high accelerations required for hard pulse characteristics of stiff vehicle structures.

The dynamic loading of the belt is generated by a free-floating mass, with the belt end being either directly attached to the mass, or with the belt being looped around the pillars mounted on the mass. The mass is accelerated by the restraining forces generated in the seatbelt like an occupant is decelerated by a SBS restraining its inertia driven forward motion in a decelerating vehicle. The subsequent detailed discussion intends to explain, how the principal dynamic boundary conditions responding to a vehicle seatbelt system under crash activation are addressed by different design elements in the bench setup, which can be adjusted to represent presumably every real-world use case.

During pretensioning phase the SBS is busy accelerating its internal components (snake, spool, webbing on spool) to pull-in the webbing, thereby sending a strain wave into the belt as discussed in appendix A and illustrated in Figure 9. This highly dynamic phase lasts only about $10\ ms$, approximately the first $7\ ms$ are needed to build up pressure in a tube, propelling a driving element, and accelerating the spool to remove coiling slack from the webbing on spool. An equivalent bench setup can be realized by providing enough belt length routed around pillars inside the frames as shown in Figure 5, as well as by providing sufficient slack to the system, being assured via a adjustable slack element. Considering that the primary function of a pretensioner is slack removal to establish early force closure of the occupant to the vehicle and to initiate the controlled occupant ride-down via the load-limiting system, consequently pretensioning into a slack-less system might be taken as a miss-use load case for real-world safety. Adjusting the total amount of available slack in the routed SBS conditions the maximum amount of webbing pull-in, and therefore, apart from the belt forces the other important parameter “spool rotation” is fixed - both together define the working point i.e., the physical straining of the pretensioner.

In the subsequent force-closure phase, which can include locking for some retractor types, forces between belt and occupant are being build-up by the relative displacement between decelerated mass (occupant) and seatbelt system whose fixation points directly follow the vehicle motion. The force closure phase is complete when reaching the first load-limiting level. Force closure phase of real-world use cases is defined by the loading rate, i.e., how fast the occupant is loading the belt and by the generated inertia force to load the retractor. Independent of the pulse applied to the moving frame the parameter can be adjusted to the real-world use case by the appropriate dynamic onset, illustrated in Figure 3 and discussed in the related section above, and by the appropriate combination of mass and load diminishing friction provided by the pillars routing and redirecting the strained webbing.

Once the load limiting level is reached dynamical effects like overshoots due to inertia/friction influence in load-limiting startup or load level switching occurring in the vehicle application can directly be studied and optimized in detail. The natural dynamic response of the mass to its activation by forces transmitted from the SBS, or vice versa the forces generated in the SBS by the activated mass, lifts dynamic bench testing of seatbelt components to the next level, as this reflects precisely what happens in a crash event.

Summary and outlook

Designed to assess dynamically seatbelt components and sub-systems with high efficiency and accuracy the Hyper Dynamic Response Actuator (HyDRA®) bench concept is presented in this paper for the very first time. The paper provides an overview of the major test setups and motivates to use generic setups, as these allow thorough control of all test and adjustment parameters, reproducing almost every relevant real-world exposure in a SBS crash activation with major back and forth loading. As a consequence, SBS functionality can be identified and validated under dynamic loads over an extended design space yielding a significant improvement in quality and in integrity of SBS.

One principal task to be accomplished is to define for each SBS product a suitable functional design space, describing, based on real-world data or on comprehensible virtual full-vehicle scenarios, the realistic dynamic exposure of the product and the required product performance. The severity of the physical stress acting on the SBS components from these type of dynamic load cases is not easy to judge - small changes in dynamics can yield drastic effects, in contrast to small changes in static loading. These corner stone scenarios naturally work in two directions: First of all they set a reference frame for SBS subsystems that enables a product performance judgement, benchmarking different variants of products, or even in comparison to alternative solutions on the market. But also it establishes a requirement to be respected for the product integration; when combining various SBS subsystems into one specific vehicle to fulfill performance aspects (occupant loading and injury risk assessment) for the full vehicle safety system. Only the strong link to real-world exposure allows to gauge all system performance aspects, and to select the technically best suited sub-system for the target vehicle.

This becomes even more important when designing future Software-Defined Adaptive Safety (SDAS) systems, that incorporate information from internal or external sensory systems into the control algorithm of the safety system. The complexity of the SDAS systems requires, as outlined in this paper, a validation with a virtual testing strategy. However, realistic advanced physical tests are compulsory to ensure that integrity and functionality of all system components is fully understood and modeled appropriately. The mentioned SBS sub-system corner stone test cases are considered as key descriptions of the SBS functionality, and the product needs to be subjected to these test cases by physically and by virtually testing in order to ensure the product performance in hardware and to demonstrate reliance of its digital functional model. The detailed presentation of such corner stone use cases, describing and illustrating specially designed SBS product characteristics, are beyond the scope of this paper and will be derived and published in subsequent publications.

The presented efficient high-accuracy dynamic test bench setups offer the opportunity not only to enhance functional robustness (quality) by performing tests with a larger sample size and with more variations in a test configuration, but they also extend the scope to identify and validate SBS functionality for new test configurations, i.e., high severity use cases or scenarios including pre-crash activation. The latter will be addressed in [12], where additional bench setups, using distributed masses of multi-body-systems to load the SBS, are presented to discuss the influence of ADAS on SBS-performance. The additional ATD like setups are geared to bridge between full vehicle setups on sleds and the high precision setups, discussed in this paper.

Acknowledgements

The authors would like to thank the entire HyDRA® project team especially Dr. Bartholomäus Brylka, Lukas Hagmanns, Jürgen Hirth, Alexander Stephan (all ZF Group), Dr. Andreas Rieser, Patrick Mayrhofer (both Humanetics Austria GmbH) and Harald Brida, Franz Unger, Dominik Kummer (all Odist GmbH) for their passion and contributions to the development of the bench. Additional thanks go to Leander Tielkes (ZF Group) and Dr. Eric Bayerschen (ZF Group) for LS-DYNA and THUMS simulation regarding the pretensioner puls validation reported in appendix A. Special thanks go to Dr. Jens Scholz (ZF Group) for extensive proof reading and his care for better text comprehensibility.

References

[1] M. Seyffert, Uwe Class: “Global Megatrends and their Impact on Occupant Safety”, Airbag 2016, 13. International Symposium, November 28-30, 2016, Mannheim, Germany, Conference proceedings: p. 35-1

[2] F. Laakmann, U. Class, O. Richard, M. Seyffert, L. Zink, P. Pedronno: “Enabling Technologies for Future Vehicles – Integrated Safety”, Airbag 2018, 14. International Symposium, November 26-28, 2018, Mannheim, Germany, Conference proceedings: V13

[3] R. Justen, M. Hermle, R. Schöneburg: “Safety is Not a Question of the Drivetrain”, VDI-Berichte Nr. 2387, page 255-270, 13. VDI-Tagung Auf dem Weg zur Fahrzeugsicherheit 2030, VDI-Verlag GmbH Düsseldorf 2022, ISSN 0083-5560, E-ISBN 978-3-18-102387-7

[4] R. W. Kent, J. L. Foreman:“Is There Really a “Cushion Effect”?: A Biomechanical Investigation of Crash Injury Mechanisms in the Obese - 2010 - Obesity - Wiley Online Library https://onlinelibrary.wiley.com/doi/full/10.1038/oby.2009.315

[5] T. Kroher:“ ADAC Crashtest: Schützen Gurte und Airbags wirklich alle Insassen?“, 2.09.2021, https://www.adac.de/rund-ums-fahrzeug/tests/crashtest/test-rueckhaltesysteme

[6] R. Reuter: „Roadmap 2030: Euro NCAP entwickelt neue Kriterien für Crashtests, https://www.automobil-industrie.vogel.de/euro-ncap-entwickelt-neue-kriterien-fuer-crashtests-a-1113849, 28.04.2022

[7] B. Rossi:”The five Ws (and one H) of effective incident response”, 23.05.2016, https://www.information-age.com/five-ws-and-one-h-effective-incident-response-123461486/

[8] H. Steffan, H. Geigl, A. Moser, M. Hofinger:”HyperG – A New Hydro Pneumatic Catapult Type Sled”, SAE Technical Paper 2003-01-0496, 2003, https://doi.org/10.4271/2003-01-0496, ISSN: 0148-7191, e-ISSN: 2688-3627

[9] Capstan equation https://en.wikipedia.org/wiki/Capstan_equation 26.01.2022

[10] H. Bock, A. Dworschak, B. Herkommer: “Gebrauchsmusterschrift DE 299 10 483 U 1”, Bekanntmachung im Patentblatt: 5.1.2000, Bundesdruckerei 11.99 902 261/87/30A

[11] H. Bock, A. Dworschak, B. Herkommer: “United States Patent No.: US006609409B1”, Aug. 26, 2003
[12] K.-U. Machens, L. Kübler: “Dynamic Testing with Pre-Crash Activation to Design Adaptive Safety Systems” accepted for oral presentation to the International Conference on Enhanced Safety of Vehicles; 2023; ID#: 23-0067, Yokohama, Japan
[13] THUMS | Toyota Motor Corporation: https://www.toyota.co.jp/thums/ 20.05.2022
[14] L. Cremer, M. Heckl: “Körperschall: physikalische Grundlagen und technische Anwendungen” ISBN 3-540-54631-6 Springer Verlag Berlin Heidelberg 1996
[15] https://de.wikipedia.org/wiki/LS-DYNA 22.02.2022
[16] http://atd-models.de/020_de_dummy-modelle.html 22.02.2022
[17] P. Hagedorn, S. Otterbein: “Technische Schwingungslehre“ ISBN 3-540-18096-6 Springer-Verlag 1987
[18] SAE Test Standard J211/1_201403: “ Instrumentation for Impact Test – Part 1 – Electronic Instrumentation” J211/1: Instrumentation for Impact Test - Part 1 - Electronic Instrumentation - SAE International
[19] D'Alembert's principle - Wikipedia: https://en.wikipedia.org/wiki/D%27Alembert%27s_principle
[20] Virtual work - Wikipedia: https://en.wikipedia.org/wiki/Virtual_work#:~:text=In%20mechanics%2C%20virtual%20work%20arises%20in%20the%20application,along%20a%20displacement%20is%20different%20for%20different%20displacements.

Appendix

A Pretensioning pulse on ATD chest

The human body consists approximately by 65% of water, consequently its surface impedance is close to the one of a water skin, and therefore the human body is acting as a mechanical low pass filter onto the load variation in the belt when the load is transmitted to deflect the sternum. This evidence is visualized the Figure 6 showing the

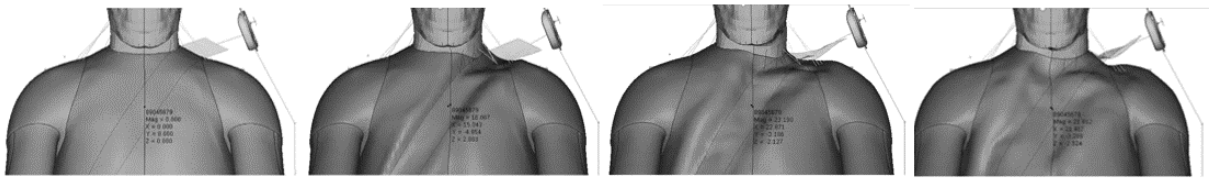

Figure 6 **Simulation of pretensioner pulse on THUMS 9 ms (far left), 16 ms (left), 24 ms (right) and 30 ms (far right) after TTF. A surface wave traveling away perpendicular to the upper body belt suggest an impedance like of a water skin. This might be regarded as a mechanical low pass filter for impact forces on the human body.**

Figure 7 **Static setup to test pretensioning pulse on THOR ATD (left picture). Illustration of IR-TRACCS (right upper picture) and position relative to belt (right lower picture) in chest region.**

simulation result of a pretensioning pulse acting onto the upper body of a Total HUman Model for Safety (THUMS) [13], with a surface wave being initiated at the contact lines between belt and virtual human body, propagating perpendicular to the belt along the chest. Pysical ATDs (Figure 7) show such a mechanical low pass filter behavior by design as well (Figure 8), a skin vest-foam-rib arrangement provides a mechanical impedance to the belt similar to the impedance generated by a human body. Consequently, only the low frequency content of the dynamically alternating load variations in the belt will be passed effectively onto the body.

Also, the sensory system to measure the sternum deflection is located inside the ATD chest behind the ribcage. In principle its local impedance is built up from sternum mass and the stiffness provided by the ribcage i.e., a simple mass-spring system. Low pass filter ATD characteristics can be experimentally demonstrated by applying a pretensioning pulse via the belt onto the ATD. When performing these tests with a THOR ATD (see Figure 7) and with an H350 ATD, local resonance frequencies f_0 as low as $\approx 45\ Hz$, and as low as $\approx 65.8\ Hz$ respectively as depicted in Figure 8, were measured.

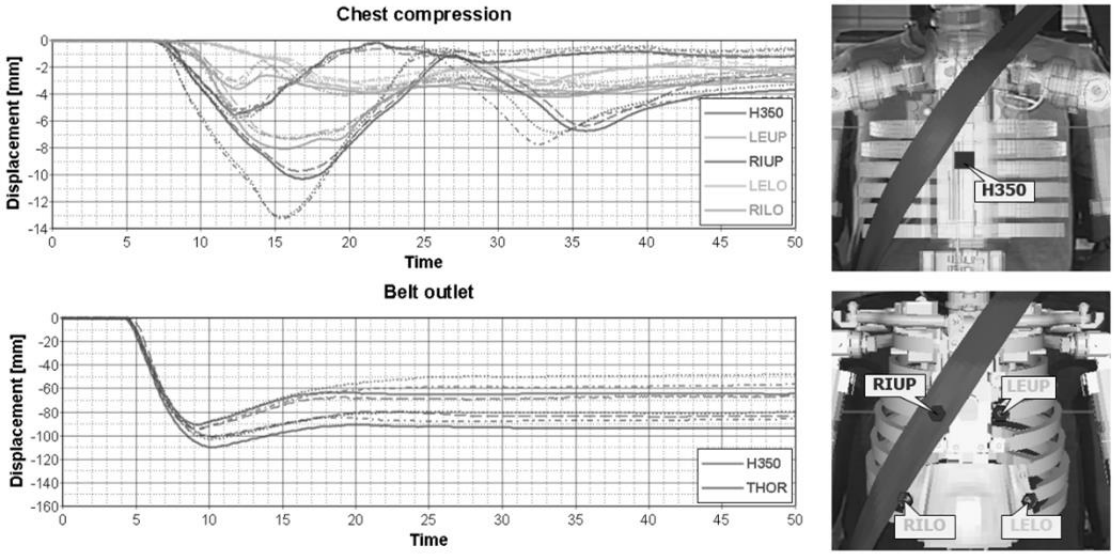

Figure 8 **Chest compression (left upper picture) and belt outlet (left lower picture) of four repetitions of pretensioning without lock pawl measured in the chest of H350 (right upper picture) and on four locations of the THOR (right lower picture). Chest displacement starts first and is larger at locations closer to the belt (RIUP) and shows up later and less pronounced at locations further away from the belt (LELO). Highest variance in the measurements at RIUP.**

The measured curves can be quite accurately predicted by the simple mechanical system illustrated in Figure 9 (left-hand side) and discussed in the following. A linear relationship between retractor force and the retractor pull-in velocity is assumed similar to the energy loss like in a viscous damper.

For an infinite linear-elastic longitudinal wave guide, initially at rest, the analytical solution of the characteristic impedance Z for longitudinal waves is known. The present case with a mass per length of $m' = 60\,\frac{g}{m}$, a cross section of $A = 56{,}4\ mm^2$ and a longitudinal stiffness of $D = 2667\,\frac{N}{mm^2}$ yields according to Cremer et al. [12] a speed of sound c_L of

$$c_L = \sqrt{\frac{D}{\rho}} = 1583\ \frac{m}{s}, \quad \text{with density } \rho = \frac{m'}{A} = 1064\ \frac{kg}{m^3} \tag{A1}$$

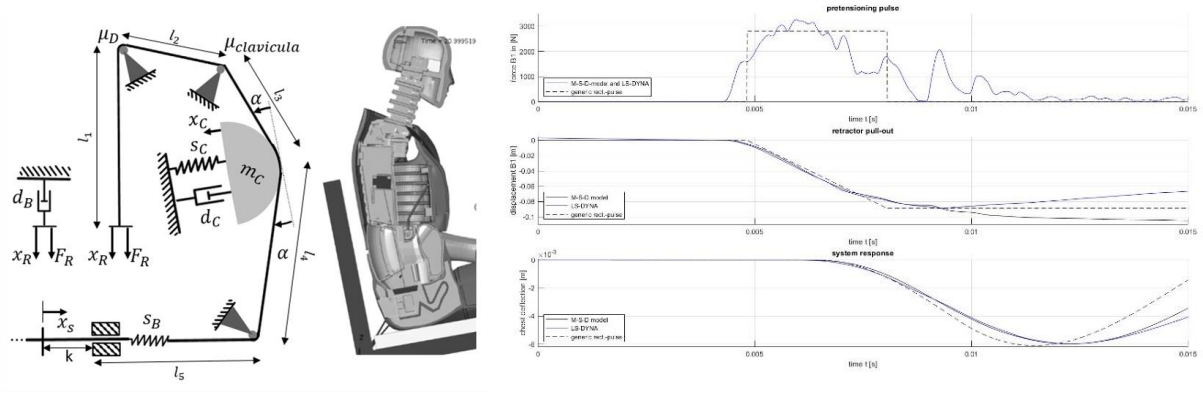

Figure 9 **left-hand picture: Basic simulation model (BSM) for pre-strain phase featuring d_B as characteristic impedance for a stress wave in an infinite belt, k the total slack length, and s_B the belt stiffness for a belt of the total length l, with chest impedance modeled as simple mass-spring-damper system. Belt friction at the D-ring and clavicula with friction coefficient μ_D and μ_{Clavi} respectively reduce the effective force on the chest dependent on the contact angle according to the capstan equation. Contact angle α determines the relation of belt force to chest deflection force. Middle picture: Negligible displace-ment of clavicula under dynamic pretensioning pulse causing a rather flat belt routing on sternum visible on LS-DYNA model. Right-hand picture: Applying the B1 force from LS-DYNA model (upper graph) to the BSM (blue line) an impressive fit to the belt pull-in (middle graph) and chest deflection (lower graph) to the ones obtained with the validated LS-DYNA model is reached. Even a simplified generic rectangular force input at B1 generates a similar system response with the BSM.**

and a longitudinal wave impedance $Z = {F_R}/{\dot{x}_R}$ resulting in a force to cross-section velocity at the retractor of

$$F_R = A\,\sigma = A\,c_L\rho\,\dot{x}_R = A\,\sqrt{D\rho}\,\dot{x}_R\,. \qquad \text{(A2)}$$

This corresponds to a constant damping coefficient $d_R = A\,\sqrt{D\rho} = 95\,\frac{kg}{s}$ establishing a linear relationship between pull-in speed and belt force. Pretensioning, designed to remove slack from the belt routing mechanism, can reach its peak force in about 3 ms after the belt pull-in started. Once the retractor spool propulsion is switched off further slack removal and elastic straining of the belt is driven by the kinetic energy stored in spool rotation velocity and belt motion. It takes about another 3 ms until inner friction in conjunction with the deceleration torque generated from the belt forces finally stop the "overrun" of the spool rotation. Naturally the gradient of belt force and hence braking torque rises rapidly as soon as all slack has been removed from the SBS system and the anchor force builds up at the fixed belt end, being fed back into the pretensioner. It shall be recalled that the information about a fixed belt end spreads in the system with the finite speed of sound according to equation (A1), and reaches the pretensioner 1.56 ms later, after having traveled along the $l = 2475\ mm$ strapped belt from anchor to retractor pretensioner. Consequently the simulated retractor force evolution with time from a validated LS-DYNA [15] model can be used to calculate with equation (A2) sufficiently accurate the belt displacement in the slack removal phase over 9 ms as illustrated in Figure 9. Forces spikes apparent in the retractor force plot after the slack removal phase i.e., after 9 ms are presumably associated to the strapped belt system responding to the pretensioning pulse.

The retractor pretension belt force wave F_R will be attenuated via friction when redirecting the webbing at the D-ring and at the clavicula by a factor of 0.635 and 0.672 respectively before it arrives at the chest. The attenuation factors are calculated by employing the capstan equation (see [9]) with friction coefficient μ_D=0.26, angle $\varphi_D = 100°$ at D-ring and μ_{Clavi}=0.35, angle $\varphi_{Clavi} = 65°$ at the chest. Clavicula inertia also provides resistance to the dynamic displacement, visualized in Figure 9 center an LS-DYNA simulation model with an ATD-H350 Modell (see [16]), yielding in a rather flat angle of about $\alpha \approx 20°$ between belt and sternum. The force signal, attenuated by a factor of

$$e^{-\mu_D \varphi_D} \cdot e^{-\mu_{Clavi} \varphi_{Clavi}} \cdot 2 \cdot \sin\alpha = 0.635 \cdot 0.672 \cdot 2 \cdot \sin 20° = 0.292, \qquad \text{(A3)}$$

is applied with a delay of $t_C = 1.7\ ms$ on a simple time invariant mass-spring-damper system representing the chest, to fit the chest displacement of the LS-DYNA model displayed on the bottom of the right-hand side graph in Figure 10. A parameter set of

$$m_C = 0.7\ kg\ , s_C = 125000\ \frac{N}{m},\ d_C = 122\ \frac{N\,s}{m} \qquad \text{(A3)}$$

can be identified, yielding a significant correlation between this simple analytical model and the measured chest deflection. The chosen delay of $t_C = 1.7\ ms$ is composed out of the strain wave travel time $t_{CB} = 0.7\ ms$ over the distance retractor to sternum ($l_1 + l_2 + l_3 = 1150\ mm$) and the transition time $t_{CC} = 1\ ms$ from skin surface displacement to sternum displacement calculated in LS-DYNA and illustrated in Figure 10.

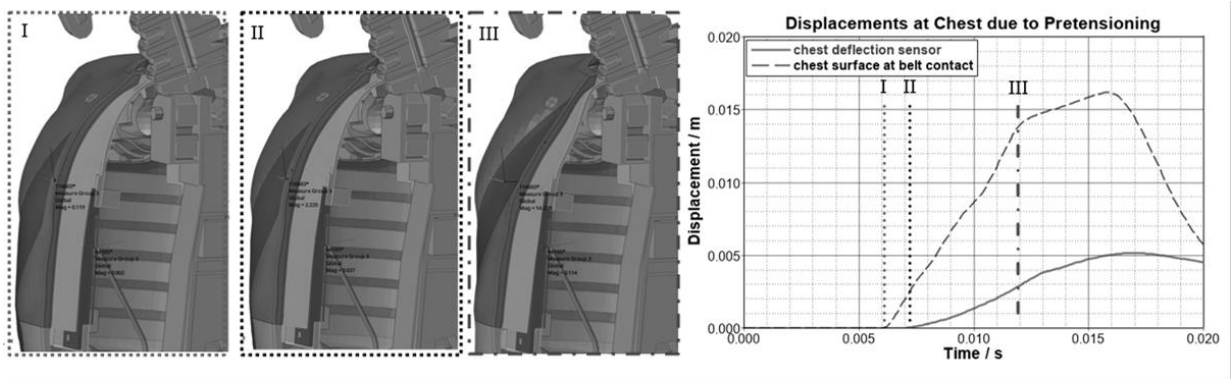

Figure 10 **LS-DYNA simulation identifies a $t_{CC} = 1\ ms$ time delay between the start of skin displacement under the belt (black dashed line) and start of sternum displacement (red continuous line) illustrated at the graph on right-hand side. Chest region deformation at 6 ms (I), 7 ms (II) and 12 ms (III) is shown in the pictures at left-hand side.**

Approximating the major pretensioning pulse by a rectangular pulse of width T_{pret} and hight F_{pret} the solution can be given analytically. This retractor force signal

$$F_R(t) = F_{pret} \cdot \Big(H(t) - H\big(t - T_{pret}\big)\Big), \text{ with } H(t) = \begin{cases} 0 & t < 0 \\ \frac{1}{2} & t = 0 \\ 1 & t > 0 \end{cases} \qquad \text{(A4)}$$

denoting H(t) the Heaviside function, travels as a strain wave which is attenuated at the deflection points and passes delayed by t_C the chest. Only the component of the strain force in upper and lower part of the chest belt, which is directed to the chest, will excite the time mass-spring-damper system

$$m_C\ddot{x}_C + d_C\dot{x}_C + s_C x_C = 0.635 \cdot 0.672 \cdot 2 \cdot \sin\alpha \cdot F_R(t - t_C) \approx 0.292 \cdot F_R(t - t_C)\,. \quad \text{(A5)}$$

In this example with $\alpha \approx 20°$ only 0.292 i.e., less than one third of the maximum belt force acts in perpendicular direction on the chest. The natural angular frequency of the mass-spring-damper in equation (A5) is calculated according to Hagedorn et al. [17] by

$$\omega = \frac{2\pi}{T} = 2\pi f = \sqrt{\frac{s_C}{m_C} - \frac{{d_C}^2}{4{m_C}^2}}\ , \qquad \text{(A6)}$$

using the parameter set in equation (A3) results in an angular natural frequency of $\omega = 414\ s^{-1}$, the period $T = 15.2\ ms$ and the natural frequency $f = 65.8\ Hz$, which is remarkably low. The analytical solution derived for example by Hagedorn et al. [17] in chapter 2.7.1 is given by

$$x_C(t) = 0.292 \cdot \frac{F_{pret}}{s_C} \cdot \left\{ H(t^*) \cdot \left[1 - e^{-\frac{d_C}{2m_C} t^*} \left[\cos \omega t^* + \frac{d_C}{2m_C \omega} \sin \omega t^* \right] \right] \right\} -$$
$$0.292 \cdot \frac{F_{pret}}{s_C} \cdot \left\{ H(t^{**}) \cdot \left[1 - e^{-\frac{d_C}{2m_C} t^{**}} \left[\cos \omega t^{**} + \frac{d_C}{2m_C \omega} \sin \omega t^{**} \right] \right] \right\} \qquad \text{(A7)}$$

having substituted $t^* = t - t_C$ and $t^{**} = t - T_{pret} - t_C$. It is indicated by the dashed line in Figure 9 and explains well the LS-Dyna Model result up to 9 ms.

The perfect match between the verified LS-Dyna model and the BSM solution starts to diverge when the belt pull-out starts as soon as the retractor pull-in force drops to almost zero at 9 ms after TTF. This emerging difference can be explained as follows: A belt with a total length $l = 2475\ mm$, assumed to be subjected to an average pretensioning force of $\bar{F}_R \approx 3kN$, will elongated according to

$$F_R = A\ D\ \frac{\Delta l}{l}, \qquad \text{(A4)}$$

such that its maximum elongation under pretentioning according to equation (A4) amounts to $\Delta l = 49\ mm$. An unlocked pretensioner will show a belt pull-out from the retractor of the same length, as its one end is fixed to the anchor and there rests apart from friction effects almost no force in the system.

Due to the low natural frequency resulting from equation (A6) , only relatively slow varying belt forces and displacements are transferred onto the ATD body as frequencies far above the resonance frequency are reduced by a $V_A = \eta^{-2}$ with $\eta = {}^{f}/_{f_0}$ being the normalized excitation frequency (see for example Hagedorn et al. [17]). Thus, only the low frequency content i.e., below $\approx 70\ Hz$ of vehicle pulses, pretensioning pulses, force peaks generated by locking or generated by switching between different load levels are going to affect the injury values measured in the ATD caused by the safety system.

Consequently, when simulating the crashworthiness for a virtual vehicle, focusing on occupant safety, only the low frequency content of anything that happens at the vehicle side of the seatbelt system needs to be incorporated into the model. This leads to more robust simulation models, as predictions of the virtual full vehicle crashworthiness restricted to the low frequency content can be computed at higher accuracy and with less effort, considering the advanced validation of the subsystem simulation models as a one time effort. Another advantage of virtual crashworthiness rating of a safety system lies in the full control of system parameters. Variations i.e., in ATD positioning, in exact belt routing, in precision at which the vehicle hits the target, along with production variability from vehicle, as well as from seatbelt components, can influence the crashworthiness and injury values. This can be eliminated in simlations, making simulations the preferred tool for safety concept development and assessment.

The mechanical lowpass filter characteristics of the ATD corresponds well to the fact that SAE Standard J211/1 [18] suggests to use Chanel Frequency Class (CFC) 60 only for vehicle structural acceleration signals when comparing full vehicles, for collision simulation input, for belt restrain system loads and for sled acceleration. On the other hand, it recommends higher Chanel Frequency Classes for subsystems. SAE Standard J211/1 states explicitly, that CFC 600 should be used for component analyses, and Anthropomorphic Test Devices (ATD) sensory system data should be processed with CFC 600-1000 to capture a potential collision with cabin elements. HyDRA® test bench is geared to capture all physical effects from the components within the CFC 600 class. Therefore, not only test bench installation including mounting subsystems and fixtures were designed to high first natural frequencies, but also for repeatability the pulse signal is closed loop controlled including the frequencies within CFC 600 characteristics. In addition, new, enhanced measurement sensors were developed in order objectively capture reliable data within the chosen filter range.

B Geometric considerations on total ATD warp angle

In this section the estimation of the total warp angle of a seat belt routed around a generic front seat passenger will be discussed, as it is important to either gauge the average force build up in the belt for holding back the ATD mass under deceleration, or to estimate the webbing pull-out of an unstrained belt deployed by an average ATD displacement.

As long as the seat belt is not tightened, the passenger will move according to Newtons first law, resulting in a forward displacement u relative to the vehicle for a frontal crash, illustrated in Figure 11. This relative ATD motion is accompanied by the belt, yielding in Δ_{po} belt payout from the retractor, and increasing the gap between passenger, seat rest and anchor points.

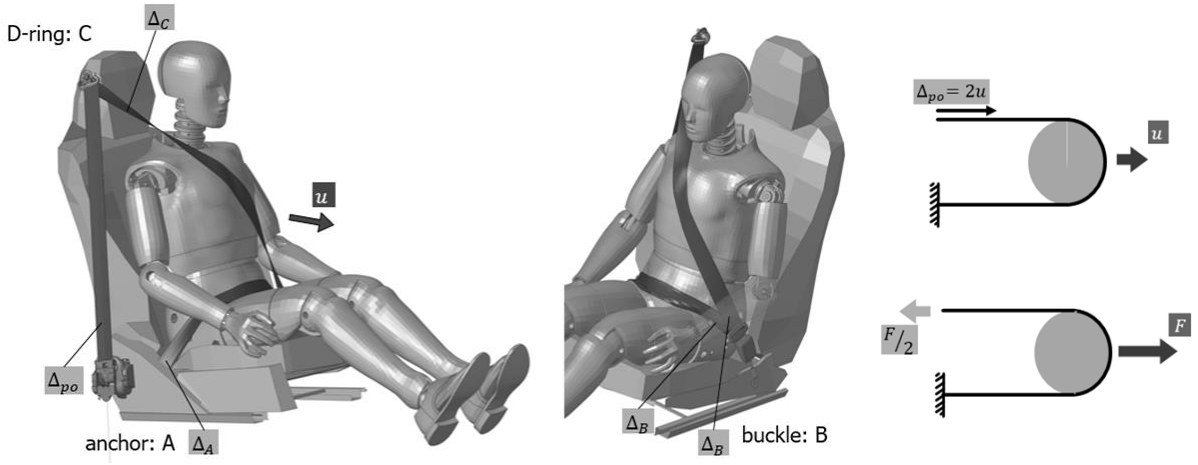

Figure 11 **Passenger displacement u relative to anchor points: D-ring, buckle, and belt anchor causes webbing payout Δ_{po} at the retractor. Example of H350-ATD viewed from right-hand and left-hand side. Right hand picture shows displacement and force relationship of a pulley resulting in half tension in belt neglecting friction between pully and belt.**

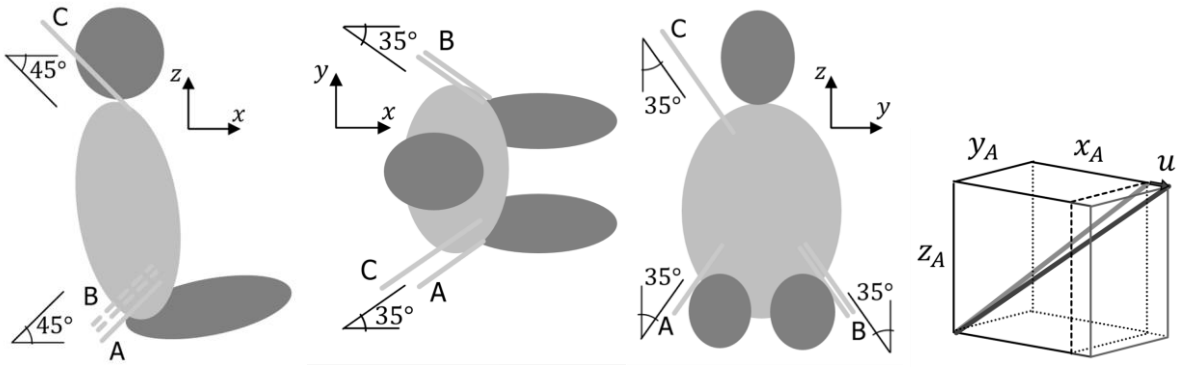

Figure 12 **Generic geometric relation to estimate webbing payout caused by passenger forward displacement relative to vehicle; picture far right: increased distance of free webbing straps due to forward displacement u**

The exact relation for the strap movement Δ_{po} as outcome of a passenger forward displacement u, depends on the coordinates of all anchor points and on the passenger size. It can be estimated via a generic geometry sketched in Figure 12 for an unstrained belt. It is assumed, that the contact between belt and ATD remains unchanged during the forward displacement, consequently the changes seen by the four free segments (Segment C: D-ring-shoulder, Segment A: Anchor – thigh, Segment B1: Buckle – thigh, Segment B2: Buckle – hip) sum up to the amount of belt removed from the retractor:

$$\Delta_{po} = \Delta_A + 2 * \Delta_B + \Delta_C \ . \tag{B1}$$

Illustrated on the right picture of Figure 12, the elongation at the belt anchor strap is defined by:

$$\Delta_A = \sqrt{(x_A + u)^2 + y_A^2 + z_A^2} - \sqrt{x_A^2 + y_A^2 + z_A^2} \ . \tag{B2}$$

When assuming small displacements equation (B2) can be simplified to:

$$\Delta_A \approx \frac{x_A \ u}{\sqrt{z_A^2 + y_A^2 + x_A^2}} \quad \text{, for} \quad u \ll \sqrt{z_A^2 + y_A^2 + x_A^2} \ . \tag{B3}$$

For the generic geometry depicted in Figure 12 with the free belt end direction

$$x_A = \sqrt{2}\, y_A = z_A \ ; \ x_B = -\sqrt{2}\, y_B = z_B \ ; \ x_C = \sqrt{2}\, y_C = -z_C \tag{B4}$$

the elongation for all four free belt segments is derived to

$$\Delta_A = \Delta_B = \Delta_C \approx \sqrt{\frac{2}{5}} u \ . \tag{B5}$$

When inserting equation (B5) into (B1) the belt elongation due to the *free* passenger motion equals the webbing pull out, and yields:

$$\Delta_{po} \approx 4\sqrt{\frac{2}{5}}\, u = 2.53\, u \ . \tag{B6}$$

When transferring this to the test setup: moving pulley as illustrated on the right-hand side top picture from Figure 11, shows that an indentical pulley displacement u will lead to 20% less webbing pull out as for the ATD buckled up on front seat load case , which is regarded as same order of magnitude. For an idealized friction-less seatbelt system the inertia force $F_{inertia}$ according to D'Alembert's principle [19] will lead to a belt force of

$$\frac{1}{2.53}\, F_R = F_{inertia} \tag{B7}$$

by using the principle of least action described in [20] and equation (B6). The looped mass used in the high precision setup discussed in this paper having the form of a moving pulley therefore corresponds sufficiently well to the kinematic condition expressed in equation (B6), experimentally simulating multibody system by a single mass.